

Reconstruction of the electronic structure in half-metallic CoS_2

R. Yamamoto, A. Machida, Y. Moritomo, and A. Nakamura

Department of Crystalline Materials Science and CIRSE, Nagoya University, Nagoya 464-8603, Japan

(Received 15 September 1998)

Temperature variation of reflectivity spectra (0.6–5.0 eV) has been investigated for ferromagnetic CoS_2 . We have found significant spectral changes at the ferromagnetic transition ($T_C=120$ K): (1) oscillator strength of the lower-lying interband transition (~ 1.6 eV) is suppressed, and (2) the higher-lying transition (~ 3.4 eV) shifts to the low energy side. We have ascribed the spectral change to the splitting of the e_g state into the up- ($e_{g\uparrow}$) and down-spin ($e_{g\downarrow}$) states, or the half-metallic behavior of CoS_2 . [S0163-1829(99)50212-9]

Strongly correlated transition-metal compounds have been attracting extensive attention. Among them, transition-metal disulfide MS_2 ($M=\text{Fe}, \text{Co}, \text{and Ni}$) shows a variety of properties: FeS_2 is a paramagnetic semiconductor, CoS_2 a metallic ferromagnet, and NiS_2 an antiferromagnetic semiconductor. Photoemission spectroscopy^{1–5} as well as the specific heat measurement⁶ indicates that these compounds have a narrow $3d$ -electron band near the Fermi level E_F . The crystal structure of these compounds belongs to the so-called pyrite type ($Pa3; Z=4$),⁷ in which divalent transition metal (M^{2+}) and sulfur dimer (S_2^{2-}) form a NaCl-like structure. Reflecting the strong crystal field due to the ligand dimers, the electron configuration of the M^{2+} ion is the low-spin state, that is, t_{2g}^6 for Fe^{2+} , $t_{2g}^6 e_g^1$ for Co^{2+} , and $t_{2g}^6 e_g^2$ for Ni^{2+} , making a sharp contrast with the perovskite-type transition-metal oxides. FeS_2 is a band insulator with a band-gap energy of 0.8 eV (Ref. 8) between the t_{2g} and e_g level, while E_F crosses the e_g band for CoS_2 and NiS_2 . The semiconductive behavior of NiS_2 has been ascribed to splitting of the e_g state by the Hubbard gap. The e_g state is strongly hybridized with the antibonding p (denote as p^*) state arising from the sulfur dimers. In CoS_2 , ferromagnetic transition takes place at $T_C=120$ K.⁹ Saturation moment is $\approx 0.86\mu_B$ per a Co site, suggesting that the itinerant e_g electrons are nearly spin polarized in the ferromagnetic state, like the doped manganite.¹⁰ A local spin density (LSD) band calculation¹¹ indicated that CoS_2 just missed being a half-metallic ferromagnetic state.

In this paper, we have investigated temperature variation of the electronic structure of CoS_2 by means of reflectivity measurements. The room-temperature reflectivity of the MS_2 series ($M=\text{Fe}, \text{Co}, \text{and Ni}$) has been measured by Suga *et al.*¹² (4–30 eV) and by Sato¹³ (0.2–4.4 eV), and the observed optical transitions have been assigned to the interband transitions in comparison with the band calculation.⁷ We have extended the investigation to lower temperature, and have found that the ferromagnetic transition induces a significant spectral change. In particular, the oscillator strength of the lower-lying transition, which has been assigned to the transition from the t_{2g} state to the e_g state, is significantly suppressed. This reduction suggests suppression of the hybridization between the e_g and p^* states. In addition, the higher-lying interband transition from the t_{2g} state to the p^* state shifts to the low energy side. We have interpreted these

results in terms of the splitting of the e_g state into the up- ($e_{g\uparrow}$) and down-spin ($e_{g\downarrow}$) states. Our observation confirms the half-metallic behavior of CoS_2 in the ferromagnetic state.

A single crystalline sample was obtained by the flux method.¹⁴ A mixture of commercial Co, S, and CoBr_2 powder (mole ratio $\text{Co}:\text{S}:\text{CoBr}_2=1:3:2$) was well ground, and was sealed into a quartz tube, 10 mm ϕ in diameter and 300 mm in length, which was evacuated with a diffusion pump. The sealed tube was heated up to 750 °C (+20 K/h) and was kept at 750 °C for 7 days. Then, the tube was slowly cooled down to 400 °C (–5 K/h) and was quenched in water. The obtained crystals were nearly black with a typical size of $2 \times 2 \times 2$ mm³. The inset of Fig. 1 shows the magnetization curve at 5 K. The magnetization steeply increases around ~ 0.1 T and reaches $\approx 0.91\mu_B$ per a Co site, which is close to the ideal value ($1.0\mu_B$). The crystal shape is polyhedral with a large (111) face, which has been used in the reflectivity measurement. Near-normal incident reflectivity measurements were made using a Fourier-type interferometer (0.05–1 eV) and a grating-type monochromator (0.6–5.0 eV). The (111) face ($\sim 1 \times 1$ mm²) was polished with a polishing sheet to a mirrorlike surface.

Before discussing the details of the temperature variation of the electronic structure, let us survey the reflectivity spectrum at 300 K. The solid curve in Fig. 1 shows the reflectiv-

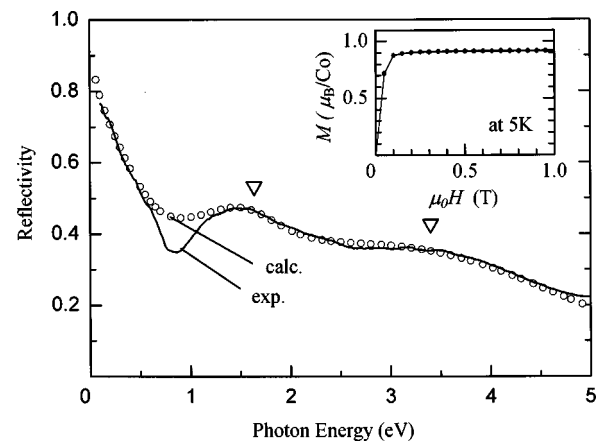


FIG. 1. Reflectivity spectrum for CoS_2 crystal measured at 300 K. Open circles represent the fitting with the Drude-Lorentz model (see text). Open triangles are the energy positions for the $t_{2g}-e_g$ and $t_{2g}-p^*$ interband transitions. The inset shows the magnetization curve at 5 K.

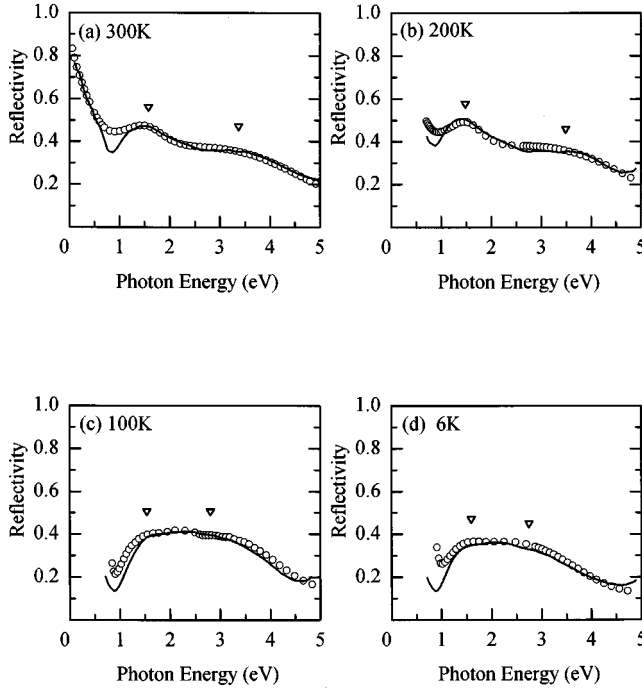


FIG. 2. Reflectivity spectra for CoS₂ together with the fitting (open circles) at various temperatures: (a) 300 K, (b) 200 K, (c) 100 K, and (d) 6 K. The open triangles represent the energy positions for the $t_{2g}-e_g$ and $t_{2g}-p^*$ interband transitions.

ity spectrum for CoS₂, which is consistent with the previous work.¹⁴ The spectrum consists of three components, that is, a Drude component below ~ 1 eV, and two interband transitions located at ~ 1.6 eV and at ~ 3.4 eV (indicated by open triangles). The lower- and higher-lying transitions have been assigned to the charge excitation from the t_{2g} state to the e_g state and p^* band, respectively.^{7,12,14} [See also the schematic density of state in Fig. 4(a).] Here, let us apply the Drude-Lorentz model to this spectra. In this model, the dielectric constant is described as

$$\epsilon(\omega) = \epsilon_\infty - \frac{\omega_p^2}{\omega(\omega + i\gamma_p)} + \sum_{l=1}^2 \frac{f_l \omega_l^2}{\omega_l^2 - \omega^2 - i\gamma_l \omega}, \quad (1)$$

where ω_l and γ_l ($l=p, 1$, and 2) are the resonance energies and damping constants for respective components. f_1 and f_2 are the oscillator strengths for the $t_{2g}-e_g$ and $t_{2g}-p^*$ interband transitions, respectively. ϵ_∞ is the background dielectric constant. The open circles in Fig. 1 are the best-fitted results; the parameters are determined as $\epsilon_\infty = 6.5 \pm 0.5$, $\omega_p = 3.6 \pm 0.1$ eV, $\omega_1 = 1.6 \pm 0.1$ eV, $\omega_2 = 3.4 \pm 0.1$ eV, $f_1 = 0.55 \pm 0.10$, $f_2 = 0.69 \pm 0.10$, $\gamma_p = 0.87 \pm 0.10$ eV, $\gamma_1 = 0.95 \pm 0.10$ eV, and $\gamma_2 = 3.5 \pm 0.5$ eV. A dip structure around ~ 1 eV is due to interference between the Drude component and the lower-lying interband transition.

Figure 2 shows the temperature variation of the reflectivity spectra: (a) 300 K and (b) 200 K are in the paramagnetic phase ($\geq T_C$), and (c) 100 K and (d) 5 K are in the ferromagnetic phase ($\leq T_C$). Well-defined peak structures are observed at 1.6 eV and 3.4 eV in the paramagnetic phase [(a) and (b)], while the structures become rather blurred in the

spin-polarized ferromagnetic phase [(c) and (d)]. This is not due to deterioration of the sample surface, because the spectral change recovers when the sample temperature rises to room temperature. We have analyzed these spectral changes with the Drude-Lorentz model [Eq. (1)], with fixed background dielectric constant ($\epsilon_\infty = 6.5$). The open triangles in Fig. 2 stand for the energy positions for the $t_{2g}-e_g$ and $t_{2g}-p^*$ transitions.

Looking at Fig. 2, one may notice that the dip structure at ≈ 1 eV deepens below T_C . This change corresponds to the reduction of the damping constant γ_p for the Drude component; the γ_p value decreases from ~ 0.9 eV at 300 K to ~ 0.01 eV at 5 K. Using the plasma frequency ω_p and its damping constant γ_p , we can roughly estimate the effective mass m^* and dc conductivity σ as

$$m^* = \frac{4\pi n e^2}{\omega_p^2} \quad (2)$$

and

$$\sigma = \frac{n e^2}{m^* \gamma_p}, \quad (3)$$

where n is the electron density ($= 2.4 \times 10^{22} \text{ cm}^{-3}$). The effective mass decreases from $\approx 2.6m_0$ (at 300 K) to $\approx 2.1m_0$ (at 5 K), while the σ value significantly enhances from $\approx 2.0 \times 10^3 \Omega^{-1} \text{ cm}^{-1}$ (at 300 K) to $\approx 2.0 \times 10^5 \Omega^{-1} \text{ cm}^{-1}$ (at 5 K). Thus estimated σ values are comparable with the experimentally determined values,¹⁵ i.e., $\approx 6.7 \times 10^3 \Omega^{-1} \text{ cm}^{-1}$ at 300 K and $\approx 3.3 \times 10^5 \Omega^{-1} \text{ cm}^{-1}$ at 5 K, indicating the properness of our analysis. If we apply the free-electron approximation, the mean free path $l (= v_F / \gamma_p$; v_F is the Fermi velocity) is estimated to be $\approx 3.1 \text{ \AA}$ (at 300 K) and $\approx 3.2 \times 10^2 \text{ \AA}$ (at 5 K). The l value at 300 K is comparable to the Co-Co distance ($= 3.8 \text{ \AA}$), suggesting the hopping-type transport dominates in the paramagnetic phase.

We plotted in Fig. 3 the obtained optical parameters for the interband transitions: (a) resonance energy ω_l , (b) oscillator strength f_l per Co site, and (c) damping constant γ_l . $l=1$ and 2 are for the $t_{2g}-e_g$ and $t_{2g}-p^*$ interband transitions, respectively. At the ferromagnetic transition, the energy difference $\Delta (= \omega_2 - \omega_1)$ between the p^* and e_g levels decreases [see Fig. 3(a)], accompanying suppression of the oscillator strength f_1 for the $t_{2g}-e_g$ transition. Note that the $t_{2g}-e_g$ transition is optically forbidden, and hence the oscillator strength should be borrowed from the higher-lying $t_{2g}-p^*$ transition through the large overlap integral t_{pd} . Therefore, the above two observations suggest suppression of the t_{pd} value in the ferromagnetic phase. Here, we adopt a simple two-level model, consisting of only the p^* and e_g levels, to the present optical transitions. With assuming $t_{pd} \approx 0$ eV at 5 K ($\Delta = 1.1$ eV), t_{pd} becomes 1.2 eV at 300 K ($\Delta = 1.8$ eV). In this model, the oscillator strength is proportional to the probability of finding the p^* state in the final state, that is, proportional to square of the coefficient of the p^* component. The ratio f_2/f_1 is estimated to be 1.5, which is close to the experimental value (≈ 1.3). Thus, the temperature-

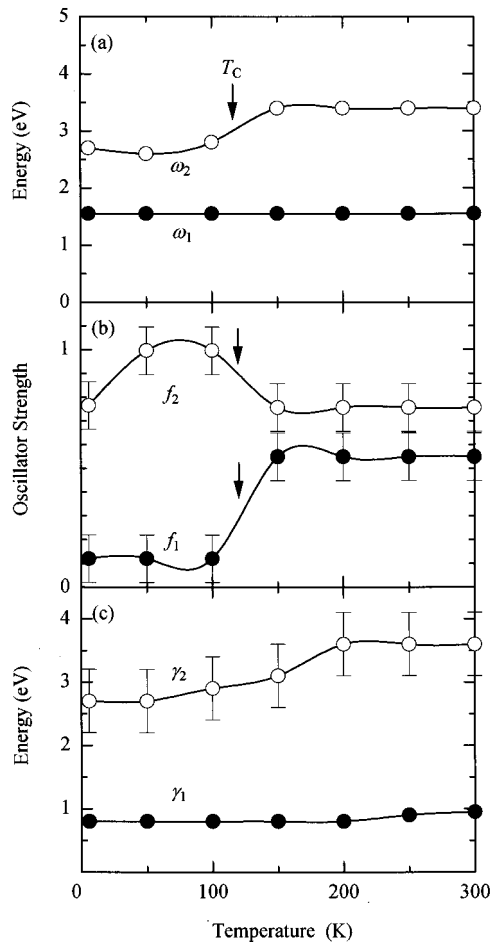


FIG. 3. Temperature dependence of (a) resonance energies ω_l , (b) oscillator strengths f_l per Co site, and (c) damping constants γ_l for the interband transitions. $l=1$ and 2 are for the $t_{2g}-e_g$ and $t_{2g}-p^*$ interband transitions, respectively. The downward arrows stand for the Curie temperature.

dependent spectral change is semiquantitatively understood as the suppression of the $p-d$ hybridization in the ferromagnetic phase.

Suppression of the $p-d$ hybridization can be ascribed to the splitting of the e_g state in the spin-polarized state. In Fig. 4 are shown schematic electronic structures for the (a) paramagnetic and (b) ferromagnetic phases. Two optical transitions denoted by ω_1 and ω_2 correspond to the $t_{2g}-e_g$ and $t_{2g}-p^*$ interband transitions, respectively. In the paramagnetic phase [Fig. 4(a)], the energy difference Δ_0 between the bare p^* and e_g levels (that is, at $t_{pd}=0$) is ~ 1.1 eV [see Fig. 3(a)]. The Δ_0 value is comparable with the bandwidths of the e_g band ($\sim 1-3$ eV),^{3,7} which causes the strong $p-d$ hybridization, as observed. In the half-metallic state [Fig. 4(b)], the $e_{g\uparrow}$ and $e_{g\downarrow}$ states are split by order of the bandwidth of the e_g band. The increased- Δ_0 between the p^* and $e_{g\uparrow}$ levels should suppress the hybridization between them [see Fig. 4(b)]. Note that the splitting of the e_g state reduces the joint density of states for the ω_1 transition, which also suppresses the oscillator strength. The spin-polarized state of the e_g

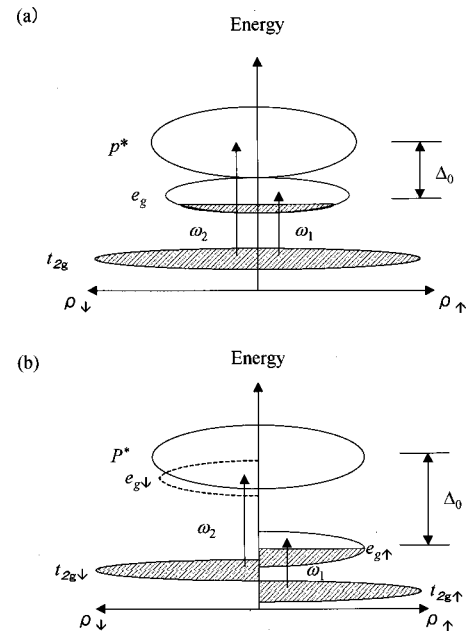


FIG. 4. Schematic electronic structure for CoS_2 in the (a) paramagnetic and (b) ferromagnetic states. Hatching represents the occupied states. ω_1 and ω_2 correspond to the $t_{2g}-e_g$ and $t_{2g}-p^*$ interband transitions, respectively.

electrons further induces the splitting of the valence t_{2g} state via the on-site exchange interaction (Hund's-rule coupling; $J_H \sim 1$ eV). On the other hand, the unstabilized $e_{g\downarrow}$ state almost merges into the p^* band, as depicted by the broken curve. This is the scenario for the reconstruction of the electronic structure in the half-metallic CoS_2 .

In summary, we have spectroscopically investigated temperature variation of the electronic structure of half-metallic CoS_2 . The observed spectral change at T_C ($=120$ K) indicates a reconstruction of the electronic structure in the perfectly spin-polarized ferromagnetic state. We have ascribed the spectral change to the splitting of the e_g state into the $e_{g\uparrow}$ and $e_{g\downarrow}$ states, and resultant suppression of the hybridization between the p^* and $e_{g\uparrow}$ states. It is suggestive to compare the electronic structure of the present CoS_2 with that of the perovskite-type doped manganites, which also becomes half-metallic in the low temperature phase. In the case of the manganites,¹⁶ the strong on-site exchange interaction between the local t_{2g} spins ($S=3/2$) and the itinerant e_g electrons *a priori* splits the e_g state by ≈ 3 eV even in the paramagnetic state. Therefore, the ferromagnetic transition does not split the energy level of the $e_{g\uparrow}$ ($e_{g\downarrow}$) state any more, but alters the occupations of the states. By contrast, the ferromagnetic transition of CoS_2 pushes down (up) the energy positions of the $e_{g\uparrow}$ ($e_{g\downarrow}$) state, which results in the spectral change observed.

The authors are grateful to K. Takenaka for his help in the reflectivity measurement in the mid-IR region. This work was supported by a Grant-In-Aid for Scientific Research from the Ministry of Education, Science and Culture, Japan.

- ¹H. S. Jarrett, W. H. Cloud, R. J. Bouchard, S. R. Bulter, C. G. Frederick, and J. L. Gillson, *Phys. Rev. Lett.* **21**, 617 (1968).
- ²E. K. Li, K. H. Johnson, D. E. Eastman, and J. L. Freeouf, *Phys. Rev. Lett.* **32**, 470 (1974).
- ³A. Ohosawa, H. Yamamoto, and H. Watanabe, *J. Phys. Soc. Jpn.* **37**, 284 (1972).
- ⁴T. Muro *et al.*, *J. Electron Spectrosc. Relat. Phenom.* **88-91**, 361 (1998).
- ⁵H. Miyauchi *et al.*, *J. Electron Spectrosc. Relat. Phenom.* **78**, 255 (1996).
- ⁶S. Waki and S. Oagawa, *J. Phys. Soc. Jpn.* **37**, 568 (1974).
- ⁷D. W. Ballett, *J. Phys. C* **15**, 6163 (1982).
- ⁸W. W. Kou and M. S. Seehra, *Phys. Rev. B* **18**, 7062 (1978).
- ⁹K. Adachi, M. Matsui, and K. Kawai, *J. Phys. Soc. Jpn.* **46**, 1474 (1979).
- ¹⁰J.-H. Park *et al.*, *Nature (London)* **392**, 794 (1998).
- ¹¹G. L. Zhao, J. Callaway, and M. Hayashibara, *Phys. Rev. B* **48**, 15 781 (1993).
- ¹²S. Suga, K. Inoue, M. Taniguchi, S. Shin, M. Seki, K. Sata, and T. Teranishi, *J. Phys. Soc. Jpn.* **52**, 1848 (1983).
- ¹³K. Sato, *J. Phys. Soc. Jpn.* **53**, 1617 (1984).
- ¹⁴K. Adachi, K. Sato, M. Okimori, G. Yamauchi, H. Yasuoka, and Y. Nakamura, *J. Phys. Soc. Jpn.* **38**, 81 (1975).
- ¹⁵S. Ogawa and T. Teranishi, *Phys. Lett.* **42A**, 147 (1972).
- ¹⁶Y. Moritomo, A. Machida, K. Matsuda, M. Ichida, and A. Nakamura, *Phys. Rev. B* **56**, 5088 (1997).